Front. Earth Sci. 2016, 10(4): 751–760
DOI 10.1007/s11707-016-0606-z

RESEARCH ARTICLE

Deformation geometry and timing of the Wupoer thrust belt in the NE Pamir and its tectonic implications

Xiaogan CHENG (✉)[1,2], Hanlin CHEN[1,2], Xiubin LIN[1,2], Shufeng YANG[1,2], Shenqiang CHEN[1,2], Fenfen ZHANG[1,2], Kang LI[1,2], Zelin LIU[3]

1 School of Earth Sciences, Zhejiang University, Hangzhou 310027, China
2 Research Center for Structures in Oil- and Gas-Bearing Basins, Ministry of Education, Hangzhou 310027, China
3 Department of Exploration Geophysics, College of Geophysics and Information Engineering, China University of Petroleum-Beijing, Beijing 102249, China

Abstract The Pamir region, located to the northwest of the Tibetan Plateau, provides important information that can aid the understanding of the plateau's tectonic evolution. Here we present new findings on the deformation geometry and timing of the Wupoer thrust belt at the northeastern margin of Pamir. Field investigations and interpretations of seismic profiles indicate that the eastern portion of the Wupoer thrust belt is dominated by an underlying foreland basin and an overlying piggy-back basin. A regional unconformity occurs between the Pliocene (N_2) and the underlying Miocene (N_1) or Paleogene (Pg) strata associated with two other local unconformities between Lower Pleistocene (Q_1) and N_2 and between Middle Pleistocene ($Q_{2\text{-}4}$) and Q_1 strata. Results of structural restorations suggest that compressional deformation was initiated during the latest Miocene to earliest Pliocene, contributing a total shortening magnitude of 48.6 km with a total shortening rate of 48.12%, most of which occurred in the period from the latest Miocene to earliest Pliocene. These results, combined with previous studies on the Kongur and Tarshkorgan extensional system, suggest an interesting picture of strong piedmont compressional thrusting activity concurrent with interorogen extensional rifting. Combining these results with previously published work on the lithospheric architecture of the Pamir, we propose that gravitational collapse drove the formation of simultaneous extensional and compressional structures with a weak, ductile middle crustal layer acting as a décollement along which both the extensional and compressional faults merged.

Received February 1, 2016; accepted August 30, 2016

E-mail: chengxg@zju.edu.cn

Keywords Pamir, Kongur, Wupoer, gravitational collapse, fold-and-thrust belt

1 Introduction

The collision between the Indian and Eurasian plates at ca. 50 Ma (e.g., Rowley, 1996) reactivated Paleozoic to Mesozoic orogenic structures (e.g., Tian Shan, Pamir, Qilian Shan, and Longmen Shan, etc.) in western China to form one of the most dramatic topographic features around the world, the Tibetan Plateau. The plateau plays a key role in our understanding of the establishment of elevated topography, topographic impacts on regional and global climate systems, processes of orogenesis and its propagation, and extensional systems within orogens.

Among these aspects, orogenic extensional systems have drawn considerable attention from global geological communities for decades. Details about the extensional system in the Tibetan Plateau have been deduced in Tibet through earthquake fault-plane solutions (e.g., Armijo et al., 1986; Mercier et al., 1987; Molnar and Chen, 1983; Molnar and Tapponnier, 1975, 1978; Ni and York, 1978; Tapponnier et al., 1986), which suggest that extensional structures are confined to the highest parts of the plateau (e.g., Molnar and Lyon-Caen, 1989; Molnar and Tapponnier, 1978; Molnar et al., 1993). These normal faults have been commonly regarded to result from gravitational collapse, marking a decrease in the mean elevation of the plateau and a release of potential energy stored in the lithosphere beneath the plateau (e.g., Molnar, 2005; Molnar et al., 1993; Molnar and Lyon-Caen, 1989; Molnar and Tapponnier, 1978). The Pamir is comparable to the Tibetan Plateau (Fig. 1(a)), with a maximum elevation of 7719 m above sea level in the Kongur Shan (Brunel et al.,

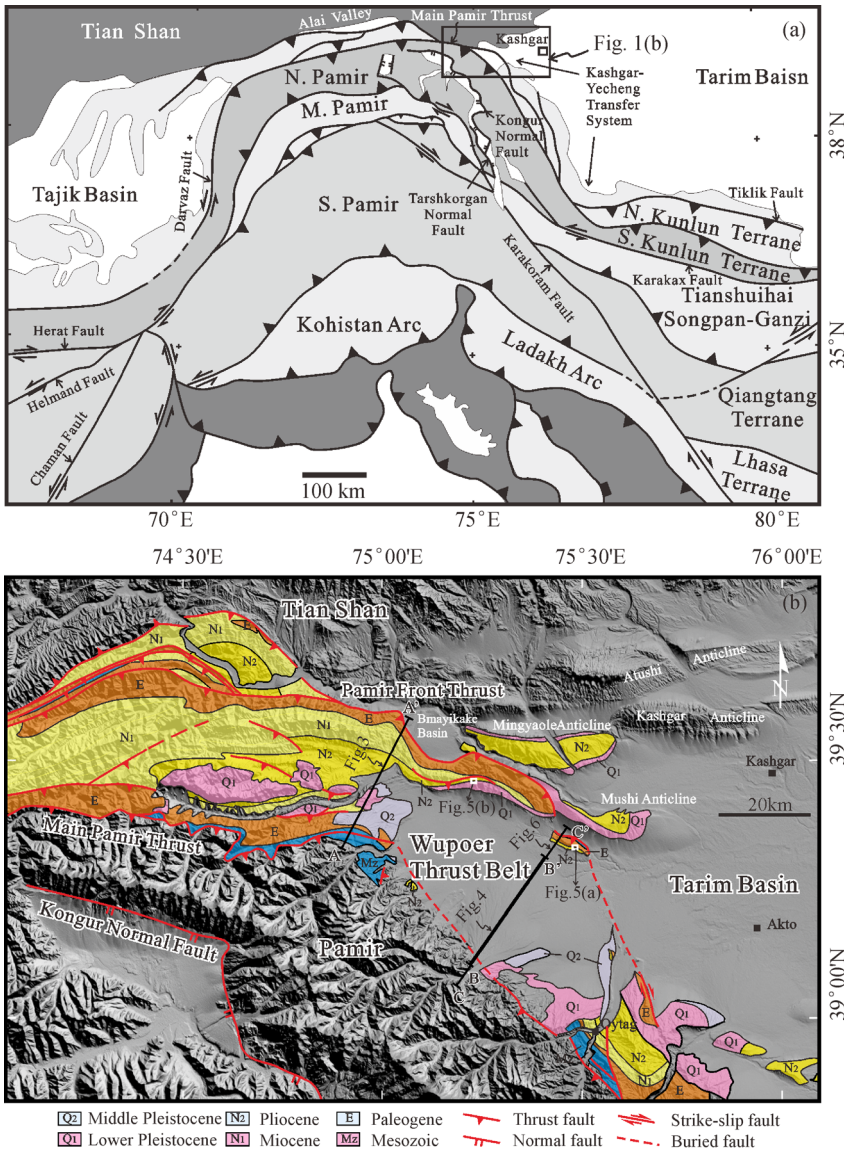

Fig. 1 Simplified map of major tectonic domains within the Pamir and simplified geologic map of the Wupoer thrust belt. (a) Tectonic setting and locality of the study area (modified from Robinson et al., 2004 and Cowgill, 2010); (b) Simplified geologic map of the Wupoer thrust belt plotted on a grey-shaded DEM image.

1994; Fu et al., 2010). N–S striking normal faults, including the Kongur normal fault and its western counterpart the Tarshkorgan fault (Fig. 1(a)), first occurred in the Pamir at ca. 8–7 Ma (Robinson et al., 2004, 2007). This resulted in the formation of the Tarshkorgan Valley, which presently has a vertical fall of more than 2000 m between the hanging wall and the footwall. This extensional system is likely to bear important information for use in understanding orogenic processes in the Pamir (e.g., Arnaud et al., 1993; Robinson et al., 2007).

Despite its significance, the driving mechanism of the Pamir extensional system remains a controversial issue (Robinson et al., 2004). Initially, the extensional system was considered to result from downward slip relative to an upward thrusting block (e.g., Arnaud et al., 1993; Brunel et al., 1994; Chemenda et al., 1995). Strecker et al. (1995), while Yin et al. (2002) emphasized the arc shape of the Pamir and proposed that the extensional system may have formed by radial thrusting or oroclinal bending. Other geologists linked the extensional system with the northwestward propagation of the dextral Karakoram fault and suggested that it was driven by strike-slip-related extension (e.g., Ratschbacher et al., 1994; Strecker et al., 1995; Murphy et al., 2000). More recently, Robinson et al. (2007) suggested a model that ties the extensional system to synchronous doming.

To address this issue, numerous efforts have been made to determine the onset timing of the extensional system.

$^{40}Ar/^{39}Ar$ dating of mylonitic rocks in the footwall of the Kongur normal fault suggests ages of 5–1 Ma, which has been regarded as the time of extension onset for the system (Arnaud et al., 1993; Brunel et al., 1994). However, these mylonitic rocks are probably associated with the Ghez fault rather than the Kongur normal fault. More recent results from multiple thermochronometers in the hanging wall and footwall of the Kongur normal fault in the Muztaghata region, including zircon U–Pb, monazite Th–Pb, and $^{40}Ar/^{39}Ar$ on several mica minerals, indicate an onset timing of ca. 8–7 Ma (Robinson et al., 2004, 2007). Other geologists, using zircon and apatite fission track and (U–Th)/He methods to determine the uplift history of different parts of the Pamir (e.g., Sobel and Dumitru, 1997; Amidon and Hynek, 2010; Sobel et al., 2011), proposed that the initial uplift likely occurred during a period earlier than the Oligocene, consistent with the work by Bershaw et al. (2012).

However, attention has rarely been paid to the piedmont deformation structures of the area. Here we present new results obtained through geologic surveying, interpretation of seismic profiles, and structural restoration in the Wupoer thrust belt in the northeastern Pamir region (Fig. 1(b)). These results indicate that the piedmont foreland of the northeastern Pamir underwent intense compressional deformation that initiated around the latest Miocene to earliest Pliocene and throughout the Quaternary period. Simultaneous occurrence of orogenic extension and piedmont compression, combined with other geophysical evidence, points to a gravitational collapse model as the origin for both the extensional and compressional structures.

2 Geologic setting

The northward-arcing Wupoer thrust belt is located in the northeastern Pamir region, bounded by the Pamir in the south, the Tian Shan in the north, the Tarim basin in the east, and the Alai basin in the west (Fig. 1(a) and (b)). The belt strikes E–W in the western portion and changes to NW–SE striking in the eastern part (Fig. 1(b)). Exposed rocks in the belt include strata from the Paleozoic to Quaternary period (regional Cenozoic stratigraphy shown in Fig. 2).

The western portion of the belt comprises, from south to north, the North Pamir fault, the Ayigaerte fault, the West Wupoer fault, and the Frontal fault, with thrust sheets in between. The North Pamir fault exposes Paleozoic strata that have been transported over Meso–Cenozoic sequences. The Ayigaerte fault exposes Jurassic to Neogene sediments that slipped northward along the fault. The West Wupoer fault comprises several thrust sheets, including Upper Cretaceous and younger strata forming southward-younging sequences. The Frontal fault represents the northernmost part of the Pamir domain, which exposes several imbricate sheets slipping northward along the detachment at the base of the Paleogene strata.

The eastern part of the belt comprises Paleozoic–Mesozoic packages, the Wupoer fault, and a piggy-back basin system. Structures adjacent to the Pamir exhibit basement-involved features and expose Paleozoic–Mesozoic sequences, which slipped northward over Cenozoic sediments. The Wupoer fault in the eastern portion has been partly exposed to the surface while part of it remains a blind fault. The hanging wall of the Wupoer fault is mainly in contact with the Paleocene Aertashi Formation. However, it also contacts Upper Cretaceous rocks discovered in the town of Wupoer, suggesting that not all of the fault plane slips along the detachment at the base of Aertashi Formation but may also slip along a deeper detachment surface.

The simplified seismostratigraphic units include pre-Mesozoic, Mesozoic, and Cenozoic units. The Cenozoic unit is the focus of this study (Fig. 2). The Cenozoic sediments contain the Paleogene Kashi Group (including the Aertashi Formation (E_1a), the Qimugen Formation ($E_{1-2}q$), the Kalataer Formation (E_2k), the Wulagen Formation (E_2w), the Bashibulake Formation ($E_{2-3}b$)), the Miocene Wuqia Group (N_1w) (consisting of the Keziluoyi Formation (N_1k), the Anjuan Formation (N_1a), and the Pakabulake Formation (N_1p)), the Pliocene Atushi Formation (N_2a), and the Quaternary Xiyu Formation (Q_1x), as well as younger deposits (Q_{2-4}) (Fig. 2). In this paper, sequences older than Mesozoic are denoted as PreMz, Mesozoic deposits are denoted as Mz, and Paleogene sediments are termed Pg (Fig. 2).

The following discussion concentrates on the eastern portion of the Wupoer thrust belt. Based on field investigations and interpretation of seismic profiles, a regional structural section was established to understand the deformation of the upper crust. Structural restoration based on a balanced section was applied to determine the deformation timing and evolution.

3 Deformation features of the Wupoer thrust belt

Based on stratigraphic divisions from drill holes, well logging, and field geology, we traced seismic reflection layers in the seismic profile network, including inlines and cross-lines, to establish interpretation models for the study area. Several representative profiles have been selected here to illustrate the deformation features, the localities of which are shown in Fig. 1(b).

In general, the study area exhibits a piggy-back basin pattern, as indicated by Section A-A' (Fig. 3). Imbricate thrust sheets formed at the southwestern end of the section. These thrust faults (faults F1, F2 and F3) carried rocks of the Paleozoic to Cenozoic ages in the hanging wall above the Quaternary sediments in the footwall of the thrust fault

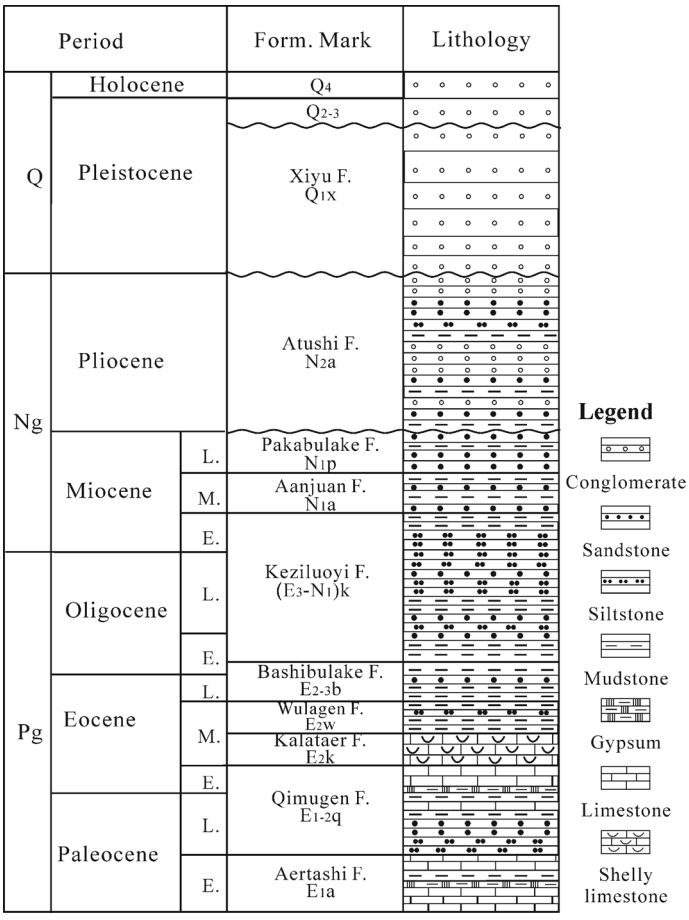

Fig. 2 Cenozoic stratigraphic units and lithology in the study area (modified from Yin et al., 2002).

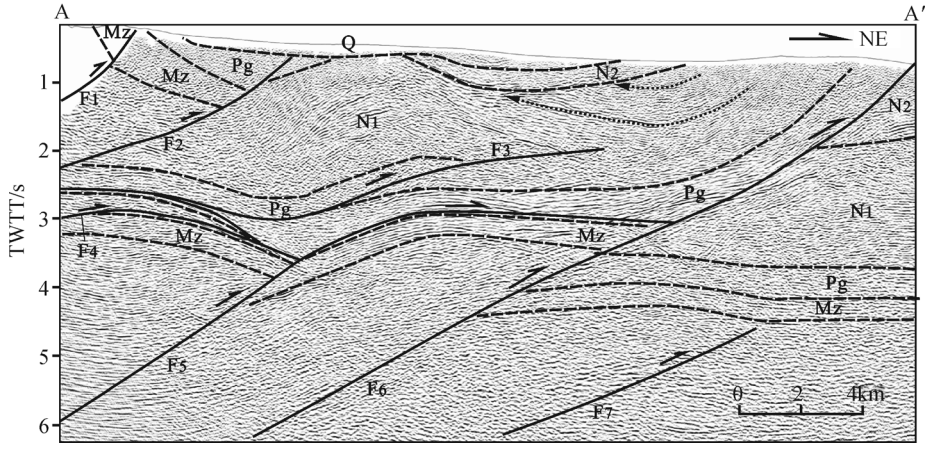

Fig. 3 Structural interpretation of seismic profile Section A-A'. The section locality is shown in Fig. 1(b). TWTT: two-way travel time.

(fault F2), where they were exhumed and exposed by erosion at the surface. This process formed the surface geology that we see today, with Paleozoic to lower Cenozoic sequences contacting the Quaternary across a thrust fault (fault F2). The Atushi Formation (N_2) thickens toward the southwest, implying that thrust fault F2 likely represents the previous boundary of the foreland basin. Several younger thrust faults (F4, F5, and F6) in the NE foreland region were then generated from F2 (likely the deeper portions of F1, F2, and F3) and broke up the basin into a piggy-back basin structure when the Wupoer fault (fault F6) developed. Another feature of the section are the

blind imbricate structures underlying the piggy-back basin, comprising thrust faults (faults F4 and F5) and their fault-bend folds. These thrust faults possibly share a roof detachment along the lowest Paleogene units (Fig. 3).

The contact between the thrust faults (F1, F2, and F3) and sedimentary sequences is clearly shown in Fig. 4. All three thrust faults (F1, F2, and F3) in the upper part of the section terminate at the bottom of the Atushi Formation (N_2a). The thickness and spatial distribution of the N_1 sequence are controlled by blind thrust faults F1, F2, and F3, which are supported by the northeastward thickening of N_1 and the absence of this sequence in the hanging walls of faults F2 and F1 (Figs. 3 and 4). N_2 was deposited above the thrust sheets of F1, F2, and F3 and formed a regional unconformity, which is also observed in field outcrops (Fig. 5(a)). In outcrop (GPS: N39°20′36.88″ and E75°26′10.45″), the $E_{2-3}b$ beds dip to 211° with a dip angle of 57°, while the overlying N_2a layers dip to 212° with a dip angle of 16°, forming a clear angular unconformity (Fig. 5(a)). Two other local unconformities in Fig. 4 are the contacts between Q_1 and N_2 and between Q_{2-4} and Q_1 sequences. Within the seismic profile (Fig. 4), part of the upper N_2 reflection layers underwent erosion and were then overlain by Q_1 sediments (Fig. 4), forming a local unconformable contact. This unconformable contact has also been observed in field outcrops (Fig. 5(b)). In an outcrop approximately 35 km northwest of the town of Wupoer (GPS: N39°26′41.67″ and E75°12′32.11″), we measured slight differences in the dip direction and dip angle between the N_2a and Q_1x sequences. The dip direction and dip angle are 170° and 43° in N_2a, which decrease to 145° and 30° in the Q_1x beds, forming a slight angular unconformity. The unconformity between the Q_{2-4} and Q_1 layers is expressed by the covering of flat-lying Q_{2-4} sequences over gently-dipping Q_1 beds. Moreover, the erosion of the Q_1 sediments in the NE and SW portions of the seismic profile Section B-B' (Fig. 4) is evident.

The regional upper crustal structure is more clearly shown in regional Section C-C' (Fig. 6), which was established based on the seismic profile B-B', regional geologic maps, and field geologic data. The southwest section is dominated by pre-Mesozoic beds that have been

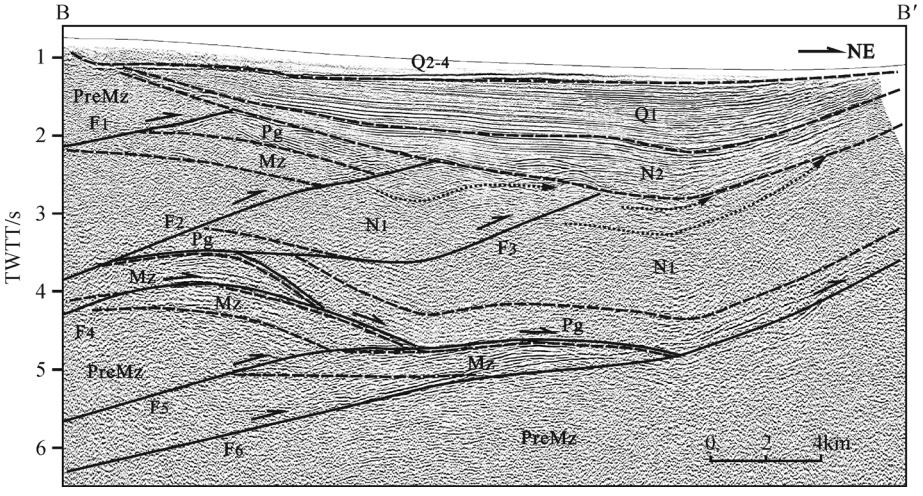

Fig. 4 Structural interpretation of seismic profile Section B-B'. The section locality is shown in Fig. 1(b).

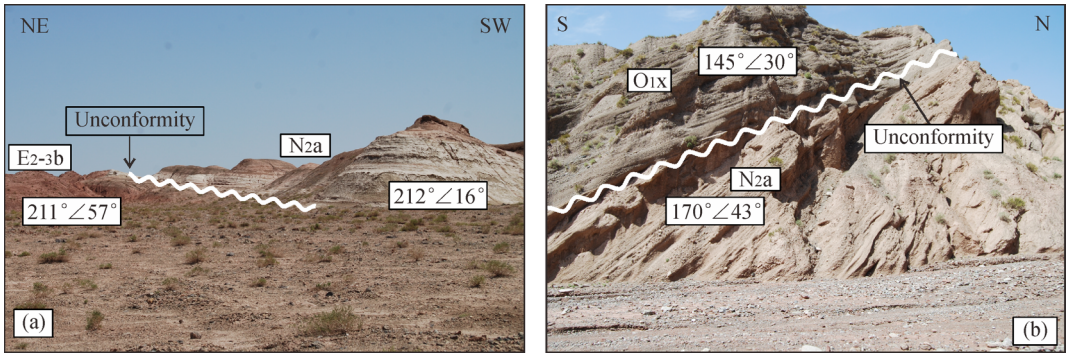

Fig. 5 Field observations of unconformities. (a) Angular unconformity between N_2a and $E_{2-3}b$ units. (b) Slight angular unconformity between Q_1x and N_2a units. The sites are shown in Fig. 1(b).

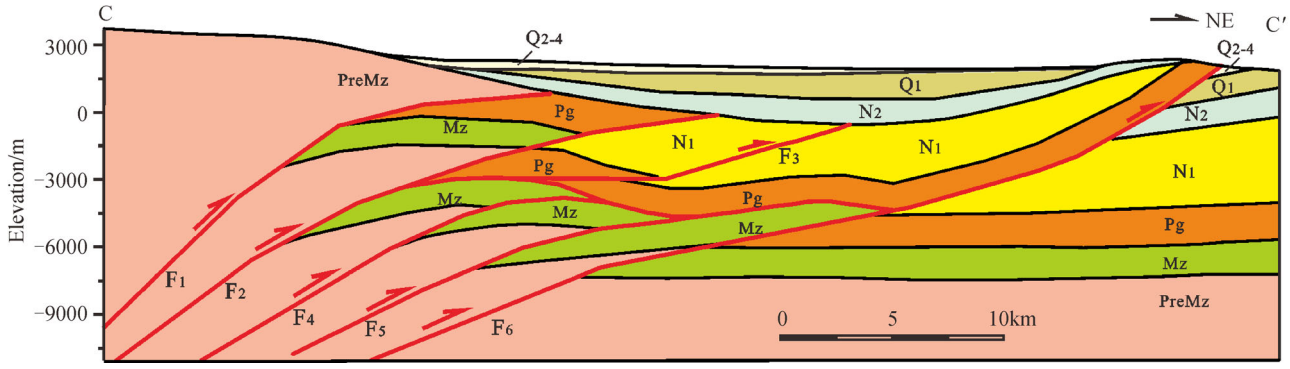

Fig. 6 Regional geologic section C-C' showing the upper crustal structure in the Wupoer region established from field data and seismic profile B-B'. The section locality is shown in Fig. 1(b).

uplifted and eroded as a result of activity on blind thrust fault F1 that terminates at the bottom of the N_2 sequence. The pre-Mesozoic beds are gradually overlapped by N_2 and Quaternary sediments toward the basin side. The middle section is characterized by a piggy-back basin, within which the N_2-Quaternary sediments overlap the pre-Mesozoic and lower Cenozoic sequences in the southwest and northeast, respectively. The piggy-back basin overlies the underlying foreland basin, which has been broken up by thrust fault activity on F3 and F6 (the Wupoer fault). Imbricate structures developed beneath the foreland basin, which comprise several thrust sheets with Mz and PreMz involved in the deformation, sharing a roof detachment along the bottom of the Cenozoic layers. The northeast end of the section is occupied by weakly deformed sequences, separated from the middle section by the Wupoer fault (F6).

4 Deformation timing and evolution

The regional deformation features provide constraints on the deformation timing of specific faults and structures by interpretations of structural relationships. The thrust fault F1 was probably the earliest to be activated among the six thrust faults, possibly before deposition of Neogene sediments, but at least before the deposition of Pliocene strata (N_2). Thrust faults F2, F3, F4, F5, and F6 were initially activated after the Miocene (N_1) and before the Pliocene (N_2), possibly forming a break-forward structural pattern, which is also supported by the piggy-back basin style. Moreover, thrust fault F6 may have experienced a longer history of activity compared with the other faults.

However, to more clearly illustrate the processes and evolution of deformation, we applied a structural restoration to regional section C-C' with balanced-section computational methods, which help evaluate the magnitude and rate of shortening (Fig. 7). A fault-slip fold model in the GeoSec software was used for the structural restoration, with the assumption that length and area remain constant. The present length of the section is 52.4 km. When restored to the period marked by the end of $Q_{2\text{-}4}$ sediment deposition, the section length increases to 55.9 km, 3.5 km larger than the present length, indicating a shortening rate of 6.26% during the end of $Q_{2\text{-}4}$. The section length increases to 63.6 km when restored to the period at the end of Q_1 strata deposition, suggesting a shortening rate of 12.11% during the end of Q_1 that formed the described unconformity between the $Q_{2\text{-}4}$ and Q_1 strata. The section length increases to 68.9 km when restored to the period at the end of N_2 sediment deposition, suggesting a shortening magnitude of 5.3 km and a 7.69% shortening rate during the end of N_2 that formed the described unconformity between the Q_1 and N_2 strata. At the end of N_1 sediment deposition, the section length was 101.0 km, indicating a shortening magnitude of 32.1 km and a 31.78% shortening rate during the end of N_1 that formed the described unconformity between the N_2 and N_1 strata. Comparison between the original undeformed and present sections suggests that the section length decreased from 101.0 to 52.4 km at present, indicating a total shortening magnitude of 48.6 km and a total shortening rate of 48.12%.

The results above suggest that regional thrust deformation was initiated during the latest Miocene to earliest Pliocene and lasted until the present. Within this time, the strongest deformation occurred during the latest Miocene to earliest Pliocene, which is supported by the occurrence of the highest shortening rates in this stage.

5 Regional tectonic implications

The new results presented in this paper indicate that the Wupoer thrust belt to the northeast of the Pamir has undergone significant compressional deformation since the latest Miocene to earliest Pliocene, forming the earlier foreland basin and the piedmont thrust sheet bounding the foreland basin, the broken foreland basin and overlying piggy-back basin, and the angular unconformities between

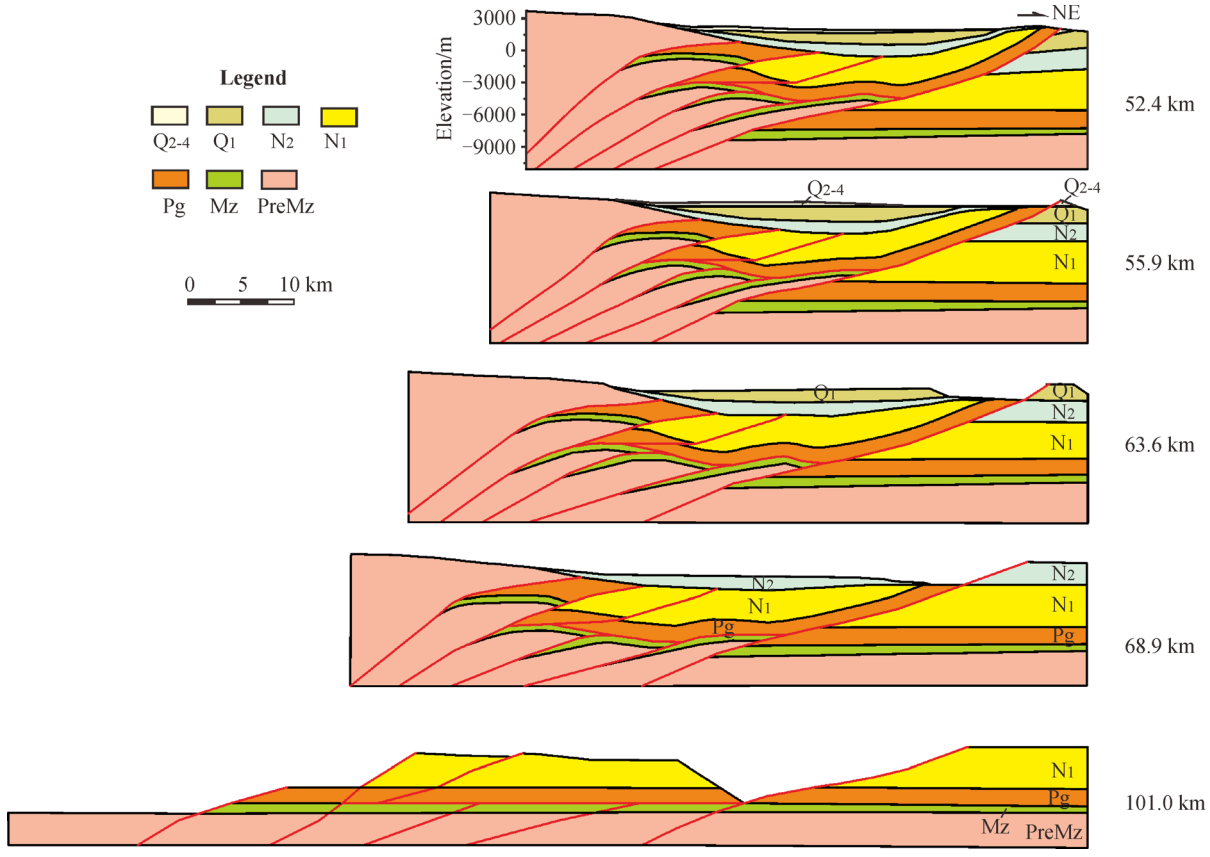

Fig. 7 Structural restoration results of regional section C-C', showing the evolution of deformation structures in the Wupoer region. The section locality is shown in Fig. 1(b).

N_2 and underlying lower Cenozoic sequences, between Q_1 and N_2 sediments and between Q_{2-4} and Q_1 strata. The structural restoration results suggest that of the 48.6 km of the total shortening, 32.1 km of this shortening occurred during the latest Miocene to earliest Pliocene, contributing 31.78% of the total 48.12% shortening rate.

Regionally, the strong thrusting and folding in the Wupoer thrust belt to the northeast of Pamir is synchronous with the onset and continued activity of the Kongur and Tarshkorgan normal faults. The Kongur normal fault was initially determined to have been activated during 5–1 Ma by $^{40}Ar/^{39}Ar$ thermochronology analysis of the samples near the Ghez fault in the footwall of the Kongur normal fault (Arnaud et al., 1993; Brunel et al., 1994). However, as continuous erosion of the footwall occurred after the inception of the extensional system, it is possible to obtain younger thermochronologic ages. The exact timing of onset should be older than 5-1 Ma. Conversely, those samples are located close to the Ghez fault and are possibly impacted by the activity of the Ghez fault rather than the Kongur normal fault, which may reduce the data reliability. More recently, Robinson et al. (2004, 2007) invoked multiple thermochronometers, including zircon U–Pb and mica mineral and monazite $^{40}Ar/^{39}Ar$ dating, to analyze the exhumation of crystalline rocks in both the hanging wall and footwall of the Kongur normal fault. A comparison of ages in the hanging wall and footwall indicates 7–8 Ma as time of onset of the extensional system activity and activity of the normal faults continuing to the present. The integrated evidence from the inner Pamir and the piedmont fold-and-thrust belt presents an interesting picture of concurrent strong piedmont compressional thrusting activity and interorogen extensional rifting.

As summarized at the beginning of the paper, several models have been proposed to explain the formation mechanism of the extensional system. The synorogenic extension model suggests that the extensional system was generated by downward slip relative to an upward thrusting block, with a similar model having been applied to interpret the Main Central Thrust in the Himalaya region (e.g., Arnaud et al., 1993; Brunel et al., 1994; Chemenda et al., 1995). This model is valid to explain the large topographic drop between the footwall and hanging wall of the normal fault, and the coexistence of compressional and extensional structures. However, there are obvious differences between the extensional system features of the Pamir and the Himalaya regions. In the Himalaya region, the extensional fault and the Main Central Thrust exhibit

parallel striking directions, consistent with the interpretation of an upward thrust-origin normal fault. In the Pamir, however, the Main Pamir Thrust presents an E–W strike, while the Kongur and Tarshkorgan normal faults strike along a S–N direction. This perpendicular relationship between the thrust and normal faults provides evidence against attributing the normal fault to upward thrusting. A model invoking northwestward propagation of the Karakoram fault to drive the occurrence of the Kongur and Tarshkorgan normal faults (e.g., Ratschbacher et al., 1994; Strecker et al., 1995; Murphy et al., 2000, Robinson et al., 2004) has been excluded by recent data. Field observations and interpretation of satellite images along the southernmost segment of the Kongur normal fault suggest that the magnitude of late Cenozoic E–W extension decreases significantly toward the south, inconsistent with the prediction (that extension magnitudes decrease northeastward) of the Karokoram fault driving model (Robinson et al., 2004). Robinson (2009) presented a new analysis of Corona and ASTER satellite images along the northern end of the Karakoram fault zone and suggested evidence against Quaternary slip on the northern segment of the Karakoram fault. These results, combined with Quaternary activity of the Kongur and Tarshkorgan normal faults, suggest that a model in which the Karakoram fault drives the extensional system is invalid. A model where radial thrusting or oroclinal bending drives the extension has been challenged by the observation of ca. 280 km of Cenozoic dextral slip along the Kashgar-Yecheng transfer system (Cowgill, 2010). Cowgill (2010) suggested that the western flank of the Pamir was accommodated by anticlockwise vertical axis rotation resulting from northwest-directed radial thrusting, while the eastern portion of the Pamir experienced transpressional strike-slip faulting. These results exclude radial thrusting or oroclinal bending in the eastern Pamir, where the Kongur and Tarshkorgan normal faults developed.

Sippl et al. (2013) used local earthquake tomography to reveal a weak and ductile middle crustal layer in the Pamir that may act as a décollement. This weak, ductile middle crustal layer may have formed during N–S-striking compression and subsequent crustal thickening (Fig. 8a). Considering the concurrent compressional and extensional deformation in the Pamir, here we instead suggest a gravitational collapse model, in which orogenic gravitational collapse drove formation of the Kongur and Tarshkorgan normal faults in the late Miocene, as well as foreland thrusting during the latest Miocene to earliest Pliocene. The ductile middle crustal layer accommodated simultaneous extension and compression, just as suggested in channel flow models (Royden et al., 1997; Clark and Royden, 2000), and the extensional and compressional faults both merged onto this décollement layer (Fig. 8b). Outward collapse of the Pamir drove strong thrusting in the foreland regions, at least in the northern, northeastern, and eastern margins of the Pamir.

6 Conclusions

Field investigations and structural interpretations of seismic profiles in the eastern portion of the Wupoer thrust belt in the NE Pamir suggest that the belt is dominated by an underlying foreland basin and an overlying piggy-back basin. A regional unconformity occurs between the N_2 beds and the underlying older layers, and two other local unconformities were discovered between Q_1 and N_2 and between the $Q_{2\text{-}4}$ and Q_1 sequences.

Structural restoration of a regional section suggests that compressional deformation was initiated during the latest

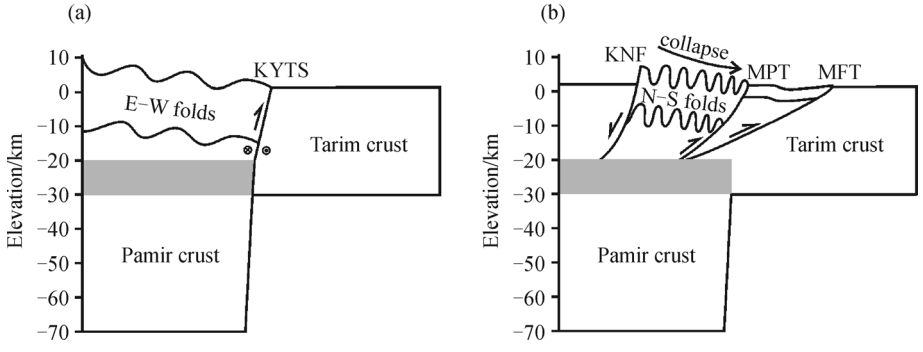

Fig. 8 Two-stage evolution of the NE Pamir. (a) Evolution of the NE Pamir before orogenic gravitational collapse. During this stage, the NE Pamir was bounded by the KYTS to the east and E–W striking folds developed in the NE Pamir. Crustal thickening resulted in the formation of a weak and ductile middle crustal layer. (b) Evolution of the NE Pamir during orogenic gravitational collapse triggered by high gravitational energy imposed by the elevated Pamir. During this stage, N–S striking folds developed between the KNF and MPT. The thrust and normal faults merged along the décollement at the weak, ductile middle crustal layer. The Tarim and Pamir crustal thicknesses and the décollement are adopted from Sipple et al. (2013). KYTS: Kashgar-Yecheng Transfer System; KNF: Kongur normal fault; MPT: main Pamir thrust; PFT: Pamir front thrust/Wupoer thrust.

Miocene to earliest Pliocene, contributing a total shortening magnitude of 48.6 km and reaching a total shortening rate of 48.12%. Most of this shortening occurred during the latest Miocene to earliest Pliocene, accounting for 32.1 km of the total shortening and 31.78% of the shortening rate.

These results, combined with previous studies on the Kongur and Tarshkorgan normal faults, indicate that strong compression in the Wupoer thrust belt at the northeast of the Pamir was temporally synchronous with the onset of activity along the Kongur and Tarshkorgan normal faults and coincident with continued activity of these faults. In combination with previously published work on the lithospheric architecture of the Pamir, we propose a gravitational collapse model as the driving mechanism for the concurrent formation of extensional and compressional structures, with a weak, ductile middle crustal layer acting as a décollement along which both extensional and compressional faults merged.

Acknowledgements We are grateful for the assistance of Lin Liao, Xiaogen Fan, Biao Bi, Xinwei Chen, Chao Chen, and Dongxu Chen during the field investigation. We received funding from National Natural Science Foundation of China (Grant Nos. 41472181, 41330207, 41102128 and 41072154), the National S&T Major Project (Grant Nos. 2016ZX05008-001 and 2016ZX05003-001), and Fundamental Research Funds for the Central University (Grant No. 2016FZA3007). We are grateful to two anonymous reviewers for their comments that improved the manuscript significantly.

References

Amidon W H, Hynek S A (2010). Exhumational history of the north central Pamir. Tectonics, 29(5): TC5017

Armijo R, Tapponnier P, Mercier J L, Han T (1986). Quaternary extension in southern Tibet: Field observations and tectonic implications. J Geophys Res, 91(B14): 13803–13872

Arnaud N O, Brunel M, Cantagrel J M, Tapponnier P (1993). High cooling and denudation rates at Kongur Shan, eastern Pamir (Xinjiang, China) revealed by $^{40}Ar/^{39}Ar$ alkali feldspar thermochronology. Tectonics, 12(6): 1335–1346

Bershaw J, Garzione C N, Schoenbohm L, Gehrels G, Li T (2012). Cenozoic evolution of the Pamir plateau based on stratigraphy, zircon provenance, and stable isotopes of foreland basin sediments at Oytag (Wuyitake) in the Tarim Basin (west China). J Asian Earth Sci, 44: 136–148

Brunel M, Arnaud N, Tapponnier P, Pan Y, Wang Y (1994). Kongur Shan normal fault: Type example of mountain building assisted by extension (Karakoram fault, eastern Pamir). Geology, 22(8): 707–710

Chemenda A I, Mattauer M, Malavieille J, Bokun A N (1995). A mechanism for syn-collisional rock exhumation and associated normal faulting: Results from physical modeling. Earth Planet Sci Lett, 132(1-4): 225–232

Clark M K, Royden L H (2000). Topographic ooze: building the eastern margin of Tibet by lower crustal flow. Geology, 28(8): 703–706

Cowgill E (2010). Cenozoic right-slip faulting along the eastern margin of the Pamir salient, northwestern China. Geol Soc Am Bull, 122 (1/2): 145–161

Fu B, Ninomiya Y, Guo J (2010). Slip partitioning in the northeast Pamir-Tian Shan convergence zone. Tectonophysics, 483(3-4): 344–364

Mercier J L, Armijo R, Tapponnier P, Carey-Gailhardis E, Lin H T (1987). Change from Tertiary compression to Quaternary extension in southern Tibet during the India-Asia collision. Tectonics, 6(3): 275–304

Molnar P (2005). Mio-Pliocene growth of the Tibetan Plateau evolution of East Asian climate. Palaeontol Electronica, 8(1): 1–23

Molnar P, Chen W P (1983). Focal depths and fault plane solutions of earthquakes under the Tibetan plateau. J Geophys Res, 88(B2): 1180–1196

Molnar P, England P, Martinod J (1993). Mantle dynamics, uplift of the Tibetan Plateau, and the Indian monsoon. Rev Geophys, 31(4): 357–396

Molnar P, Lyon-Caen H (1989). Fault plane solutions of earthquakes and active tectonics of the Tibetan Plateau and its marigins. Geophys J Int, 99: 123–153

Molnar P, Tapponnier P (1975). Cenozoic tectonic of Asia: Effects of a continental collision. Sciences, 189: 419–426

Molnar P, Tapponnier P (1978). Active tectonics of Tibet. J Geophys Res, 83(B11): 5361–5375

Murphy M A, Yin A, Kapp P, Harrison T M, Ding L, Guo J H (2000). Southward propagation of the Karakoram fault system, southwest Tibet: Timing and magnitude of slip. Geology, 28(5): 451–454

Ni J, York J E (1978). Late Cenozoic tectonics of the Tibetan Plateau. J Geophys Res, 83(B11): 5377–5387

Ratschbacher L, Frisch W, Liu G, Chen C C (1994). Distributed deformation in southern and western Tibet during and after the India-Asian collision. J Geophys Res, 99(B10): 19917–19945

Robinson A C (2009). Evidence against Quaternary slip on the northern Karakorum fault suggests kinematic reorganization at the western end of the Himalayan-Tibetan orogen. Earth Planet Sci Lett, 286(1-2): 158–170

Robinson A C, Yin A, Manning C E, Harrison T M, Zhang S H, Wang X F (2004). Tectonic evolution of the northeastern Pamir: Constraints from the northern portion of the Cenozoic Kongur Shan extensional system, western China. Geol Soc Am Bull, 116(7/8): 953–973

Robinson A C, Yin A, Manning C E, Harrison T M, Zhang S H, Wang X F (2007). Cenozoic evolution of the eastern Pamir: Implications for strain-accommodation mechanisms at the western end of the Himalayan-Tibetan orogen. Geol Soc Am Bull, 119(7/8): 882–896

Rowley D B (1996). Age of initiation of collision between India and Asia: a review of stratigraphic data. Earth Planet Sci Lett, 145(1-4): 1–13

Royden L H, Burchfiel B C, King R W, Wang E C, Chen Z L, Shen F, Liu Y P (1997). Surface deformation and lower crustal flow in eastern Tibet. Science, 276(5313): 788–790

Sippl C, Schurr B, Tympel J, Angiboust S, Mechie J, Yuan X, Schneider F M, Sobolev S V, Ratschbacher L, Haberland C (2013). Deep burial of Asian continental crust beneath the Pamir imaged with local earthquake tomography. Earth Planet Sci Lett, 384: 165–177

Sobel E R, Dumitru T A (1997). Thrusting and exhumation around the margins of the western Tarim basin during the India-Asia collision. J

Geophys Res, 102(B3): 5043–5063

Sobel E R, Schoenbohm L M, Chen J, Thiede R, Stockli D F, Sudo M, Strecker M R (2011). Late Miocene-Pliocene deceleration of dextral slip between Pamir and Tarim: Implications for Pamir orogenesis. Earth Planet Sci Lett, 304(3-4): 369–378

Strecker M R, Frisch W, Hamburger M W, Ratschbacher L, Semiletkin S, Zamoruyev A, Sturchio N (1995). Quaternary deformation in the Eastern Pamirs, Tadzhikistan and Kyrgyzstan. Tectonics, 14(5): 1061–1079

Tapponnier P, Peltzer G, Armijo R (1986). On the mechanics of the collision between India and Asia, in Collision Tectonics, edited by M P Coward and A C Ries, Geological Society of London, London: 115–157

Yin A, Robinson A, Manning C E (2001). Oroclinal bending and slab-break-off causing coeval east-west extension and east-west contraction in the Pamir-Nanga Parbat syntaxis in the past 10 m.y.. In: AGU Fall Meeting 2001, Abstracts, Vol 1 San Francisco: AGU, 03

Yin A, Rumelhart P E, Butler R, Cowgill E, Harrison T M, Foster D A, Ingersoll R V, Zhang Q, Zhou X Q, Wang X F, Hanson A, Raza A (2002). Tectonic history of the Altyn Tagh fault system in northern Tibet inferred from Cenozoic sedimentation. Geol Soc Am Bull, 114 (10): 1257–1295